The hidden life of cosmic carbon

Infrared fingerprint spectroscopy and fragmentation chemistry of gas-phase polycyclic aromatic hydrocarbons

Wiersma, S.D.

Publication date
2021

Chapter 2

Methods

PAHs appear in numerous interstellar environments, and play a significant role in the chemistry of the ISM. Laboratory experiments can be used to record their infrared absorption spectra and explore the way PAHs behave after exposure to intense light exposure. Such experiments are crucial to determine the validity of theoretical models, and provide the foundation for interpreting astronomical observations.

In this Chapter, the mass spectrometric and infrared spectroscopic techniques are described that are used to study the vibrational spectroscopy and fragmentation chemistry of gas-phase PAHs. First, the principles behind Fourier Transform Ion Cyclotron Resonance Mass Spectrometry (FT-ICR) are explained, after which the ultraviolet (UV) dissociation and InfraRed Multiple Photon Dissociation (IRMPD) are discussed. The last part of this Chapter is dedicated to a short introduction to Density Functional Theory (DFT), the method used for the theoretical calculations in this thesis.

2.1 Mass spectrometry

The detection of fragment ions is central to the action spectroscopy technique used in this work. For this, Fourier Transform Ion Cyclotron Resonance (FT-ICR) mass spectrometry was used [135]. This technique uses magnetic fields to induce circular motion of ions, for which the orbital frequency, called the cyclotron frequency ω_c, is a function of its mass-to-charge ratio (m/z). Ion packets that move close to a metal surface can be detected through the image current generated by these ions. If this signal is Fourier transformed, ions of a certain m/z ratio are revealed through a band in frequency space.

In a spatially uniform magnetic field $\vec{B}$, an ion with charge z and velocity $\vec{v}$ is subject to the Lorentz force $\vec{F}_l$:

$$\vec{F}_l = z\vec{v} \times \vec{B}. \tag{2.1}$$

This cross product dictates that the force is both perpendicular to the particle's velocity and the magnetic field, creating a stable circular orbit, called a cyclotron orbit. To find the associated cyclotron frequency ω_c, we equate the Lorentz force to the centrifugal force:

$$zvB = m\frac{v^2}{r}, \quad \omega = v/r, \tag{2.2}$$

$$\omega_c = \frac{zB}{m}. \tag{2.3}$$

Equation 2.3 reveals that the cyclotron frequency ω_c is inversely proportional to m/z. The radius of the orbit, which determines the amplitude of the detected image current, can be derived from these equations using the thermal velocity. This thermal velocity equals $v = \sqrt{2k_BT/m}$ in any single direction for a particle in equilibrium with its environment. We thus find for the unperturbed cyclotron orbit:

$$r_c = \frac{\sqrt{2mk_BT}}{zB}. \tag{2.4}$$

A typical FT-ICR measurement cell consists of four parts: an entrance, an exit, excitation plates and detection plates. The entrance and exit are open in the middle to allow ions and laser light to enter. In the illustrations in Fig. 2.1, a typical setup is shown. Here, the six-step sequence necessary for the measurement of photofragmentation is detailed, which is the type of experiment this thesis focuses on. First, the trap needs to be emptied (1). To this end, the entrance electrode is set to a positive potential, while the exit is set to a negative potential, thereby extracting the remnant sample from the previous measurement cycle. The new sample of gas-phase cations is then loaded into the cell (2) by setting the entrance to a zero potential and the exit to a positive one.

The stored sample usually contains several masses, often consisting of contaminations or unwanted isotopes. Each mass has its own cyclotron orbit, as the cyclotron frequency

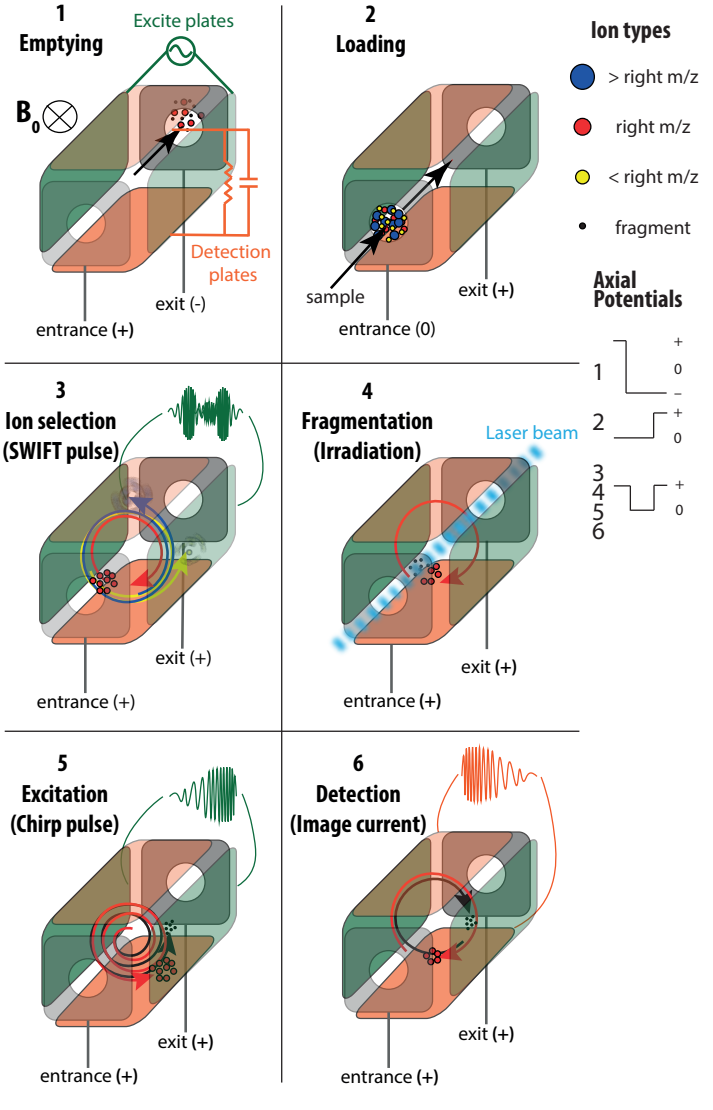

FIGURE 2.1: Illustrations of an ICR cell, going through a typical measurement cycle for photodissociation experiments in an FT-ICR cell. End caps are displayed in gray, excite plates in green and detect plates in orange. A simple sketch of the axial potentials and the particle color schemes are given in the legends on the right.

is a function of mass (see Equation 2.4). The orbits for three different masses are depicted in step (3). The red particles are those of interest, the blue ones are too heavy, and the yellow ones are too light. The masses that are not of interest can be removed using a stored waveform inverse Fourier transformation (SWIFT) pulse [136]. An electric, radio-frequency (rf) field is applied between the two opposing excite plates, depicted in green in Fig. 2.1, panel (3). By applying a $V_0 \cos(\omega t)$ between the two opposing excitation plates, the rotating ions experience opposing $-V_0 \cos(\omega t)$ and $+V_0 \cos(\omega t)$ rf potentials. If frequency ω equals ω_c, this process pushes the ions out of their initial orbit, making them move closer to the excite/detect plates without breaking up the ion packets. With prior knowledge of the contaminant masses (blue and yellow ions), an inverse FT to selected portions of the mass spectrum is applied, selectively exciting the unwanted masses into orbits outside of the cell.

In the case of PAHs, impurities are often produced in the vaporization or ionization process. The necessary excitation can cause fragmentation [88, 137–139], and high initial densities can lead to clustering. Furthermore, PAHs naturally occur with a significant amount of ^{13}C isotopes, which could for instance obscure losses of [H] versus [2H]. The removal of these isotopologs is thus of the utmost importance. After the SWIFT pulse, only a pure sample of "red" ions is left behind, ready to be irradiated, as depicted in Fig. 2.1, panel (4). Photodissociation results in one or several charged fragments which will have smaller orbits, here presented in black.

After irradiation, the sample is mass-analyzed. All orbits need to be increased such that the ions pass close to the detect plates, inducing a measurable image current. This is achieved by applying a broadband frequency-sweeping excitation, a chirp, on the excite plates. This is depicted in Fig. 2.1, panel (5), where the red and black masses both follow their own orbit close to the excite/detect plates. The decay of these orbits is measured as an envelope of damped alternating currents, called a time transient (6), which can be Fourier transformed to frequency space, after which it is converted to a mass spectrum using Equation 2.3.

2.2 Infrared spectroscopy

Infrared lines such as the AIBs are a direct probe of the vibrations between atoms in a molecule and many functional groups possess characteristic vibrational frequencies. For example: C–H stretch modes are found at 3.3 μm [32], C–H out-of-plane bends for PAHs with two or three peripheral hydrogens at 10.5–13.5 μm [43] and structure-sensitive skeletal vibrations beyond 20 μm [140]. These vibrations can be modeled as harmonic vibrations of a spring, where the spring constant k depends on the binding energy. For the sake of simplicity, we will first limit ourselves to a diatomic molecules with atomic masses m_1 and m_2. For this example, Hooke's law can be used to give the potential $V(x)$:

$$V(x) = \frac{1}{2} k x^2. \tag{2.5}$$

With μ as the reduced mass of the system, and one mass-weighted displacement x for both atoms, this classical, parabolic potential can be put into the Schrödinger equation (SE):

$$\mu = \frac{m_1 m_2}{m_1 + m_2}, \tag{2.6}$$

$$x = \frac{m_1 x_1 + m_2 x_2}{m_1 + m_2}, \tag{2.7}$$

$$E\Psi(x) = \frac{-\hbar^2}{2\mu}\frac{d^2\Psi(x)}{dx^2} + \frac{1}{2}kx^2\Psi(x). \tag{2.8}$$

Solving for the energy and the wave function [141] then yields:

$$E_n = h\nu\left(n+\frac{1}{2}\right) = \hbar\sqrt{\frac{k}{\mu}}\left(n+\frac{1}{2}\right), \tag{2.9}$$

$$\nu = \frac{1}{2\pi}\sqrt{\frac{k}{\mu}}, \tag{2.10}$$

where ν is the frequency of the oscillation and $n = 0, 1, 2\ldots$ the vibrational quantum number. The parabolic potential, and the equidistant rungs of the vibrational ladder, are depicted in the left curve of Fig. 2.2. Here, it is clearly shown that E_0 is not the bottom of the curve, but is slightly raised above it, giving the molecule a zero-point energy. D_0 and D_e are different ways to define dissociation energies, D_e is defined from the bottom of the well, while D_0, the energy needed for dissociation, is defined from the zero-point energy level. The dependence on μ is important when isotopes are considered. Not only can the inclusion of an isotope shift vibrational frequencies, the dissociation energies will also be affected.

In many cases, the harmonic model provides an adequate description of vibrational motion. However, an ever-increasing restoring force as the distance between the atoms becomes bigger is unphysical. A commonly used potential for a more accurate description is the Morse potential, which is given on the right hand side in Fig. 2.2 [142]. The shape of this well is described by:

$$V(x) = D_e\left(1 - e^{-\sqrt{k/2D_e}(x-x_0)}\right)^2, \tag{2.11}$$

in which x_0 is the equilibrium distance between the atoms, and D_e is the depth of the well. The solution of the SE with this potential leads to the following formula for the energy levels in the Morse model:

$$E_n = h\nu\left(n+\frac{1}{2}\right)\left(1 - \chi\left(n+\frac{1}{2}\right)\right), \tag{2.12}$$

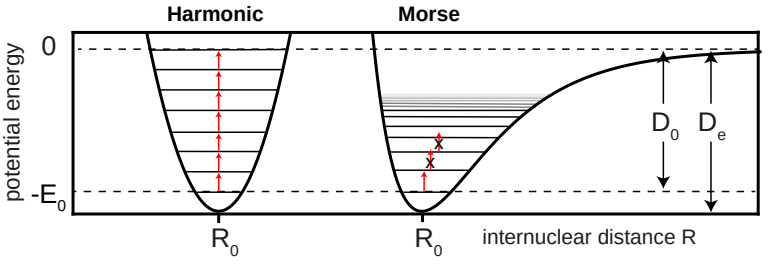

FIGURE 2.2: Comparison of the harmonic potential and Morse potential, as a function of the internuclear distance R. The horizontal lines in both wells depict the vibrational energy levels, which are equidistant in the harmonic well and become increasingly dense for higher energies in the Morse well.

in which χ is the anharmonicity constant, accounting for the increasingly dense ladder spacing. The derivation for a polyatomic molecule is more complicated, but yields analogous results. The following is a brief summary of the detailed derivation in Demtröder [118], for which we first return to the harmonic approximation.

In a molecule consisting of N atoms, $R = \{R_l\}$ with $\{l = 1,\ldots,N\}$ denotes the nuclear coordinates. Assuming a well-established geometry for the ground state, an equilibrium coordinate R_0 is defined. To find vibrational eigenstates, we have to solve for minima in the potential. To this end, a second-order Taylor approximation for the vibrational potential is made:

$$V(R) = V(R_0) + \sum_{l=1}^{3N} \frac{\partial V}{\partial R_l}(R_l - R_0) + \frac{1}{2}\sum_{l=1}^{3N}\sum_{m=1}^{3N} \frac{\partial^2 V}{\partial R_l R_m}(R_l - R_0)(R_m - R_0). \qquad (2.13)$$

The first term is constant and does not need to be considered. For a stationary point ($\nabla V = 0$), the second term reduces to zero. Furthermore, the coordinates can be defined arbitrarily, which is why we can set R_0 to zero, which leaves only the quadratic term:

$$V^{(2)}(R) = \frac{1}{2}\sum_{l=1}^{3N}\sum_{m=1}^{3N} \frac{\partial^2 V}{\partial R_l \partial R_m} R_l R_m. \qquad (2.14)$$

This is where we introduce a $3N \times 3N$ matrix $\hat{K}$, which contains the vibrational force constants k_{lm}. By simultaneously introducing mass-weighted normal coordinate vectors, $\vec{Q}$, the differential equations are uncoupled, yielding:

$$k_{lm} = \frac{\partial^2 V}{\partial Q_i \partial Q_j}, \tag{2.15}$$

$$\hat{V} = \vec{Q}^{\dagger} \hat{K} \vec{Q}, \tag{2.16}$$

$$E_i = h\nu_i \left(n + \frac{1}{2} \right). \tag{2.17}$$

This closely reproduces the harmonic solution that was also found for diatomic molecules, with a quantum number n describing the energy level. In the case of symmetric molecules, some of the vibrations are degenerate, resulting in less than $3N-6$ vibrational frequencies. The frequencies $\nu = \{\nu_i\}$ with $\{i = 1, 2, \ldots, 3N-6\}$ are the eigenfrequencies for a specific vibration i.

Although this harmonic approximation works well, the $(3N-6)$ dimensional potential for polyatomic molecules is anharmonic too. For anharmonic approximations, couplings between different vibrational modes needs to be included, which leads to non-equidistant energy levels. The deviation from the harmonic model also breaks the dipole selection rules, allowing for IR excitation of overtones ($n = 0, \nu_i \rightarrow n = 2, \nu_i$), or combination modes, wherein two different vibrations are excited together with one photon $(n = 0, \nu_i + n = 0, \nu_j) \rightarrow (n = 1, \nu_i + n = 1, \nu_j)$. To accommodate the couplings between different modes, anharmonic frequency calculations include the cubic and quartic terms of the Taylor expansion [143]:

$$\hat{V}^{(3)} = \frac{1}{6} \sum_{l=1}^{3N} \sum_{m=1}^{3N} \sum_{n=1}^{3N} \frac{\partial^3 V}{\partial R_l \partial R_m \partial R_n} R_l R_m R_n, \tag{2.18}$$

$$\hat{V}^{(4)} = \frac{1}{24} \sum_{l=1}^{3N} \sum_{m=1}^{3N} \sum_{n=1}^{3N} \sum_{o=1}^{3N} \frac{\partial^4 V}{\partial R_l \partial R_m \partial R_n \partial R_o} R_l R_m R_n R_o. \tag{2.19}$$

For polyatomic molecules, we assume that the well shapes for the individual modes ν_i are similar to those in Fig. 2.2. In a harmonic well, it would be possible to climb the ladder with photons at a single frequency $n = 0 \rightarrow n = 1$, and reach an ionization or fragmentation level ($n = 0 \rightarrow n = 1 \rightarrow n = 2 \ldots$). In the anharmonic well, this is no longer possible, because the $n = 1 \rightarrow n = 2$ transition has a different energy — which is generally lower — than the $n = 0 \rightarrow n = 1$ transition. This effect, commonly referred to as the anharmonicity bottleneck [124], is illustrated in the right panel of Fig. 2.2 by the red, vertical arrows.

2.2.1 Infrared multiple photon dissociation

To circumvent the anharmonicity bottleneck, the IR spectra in this thesis are measured using infrared multiple photon dissociation (IRMPD) spectroscopy. Combined with a high-power free-electron laser, it is possible to scan long ranges in short amounts of time, and

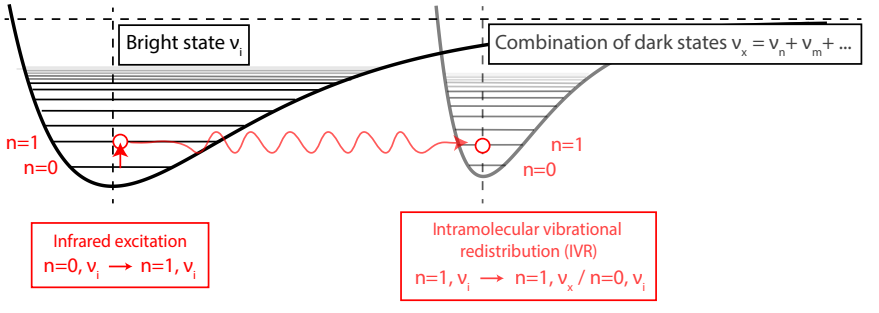

FIGURE 2.3: Simple model for IVR after resonant IR excitation. The energy from the $n = 0, \nu_i \rightarrow n = 1, \nu_i$ coordinate is funneled towards a superposition of several, anharmonically coupled states $n = 1, \nu_x$, which amount to the same energy. This leaves the initial vibrational ground state open $(n = 0, \nu_i)$ for sequential absorption.

measure low-frequency modes of gas-phase, bare molecules down to 100 cm^{-1}/100 μm. Furthermore, photodissociation is not just a means to an end; instead, fragmentation also provides valuable information in the quest for a better understanding of the processes occurring in PAHs under the influence of harsh interstellar conditions.

Due to the anharmonic coupling between different normal modes, the energy deposited in a particular vibrational coordinate ν_i can be transferred to another coordinate ν_j within nanoseconds, via intramolecular vibrational redistribution (IVR) [144–146]. In Fig. 2.3, the IVR principle is displayed. Absorption of a resonant IR photon populates, for example, the $n = 1$ level of a particular vibration ν_i. This level is embedded in a bath of 'dark' background levels ν_j involving excitations of other, lower-energy, vibrational modes. Anharmonic couplings between the 'bright' excited level of vibration and these 'dark' levels result in the transfer of the population from the 'bright' to the 'dark' states. This opens up the ground state of ν_i again, allowing the molecule to absorb an additional, resonant infrared photon. This process can be repeated until the energy absorbed by the molecule is such that the dissociation level – D_0 – is reached (see Fig. 2.2), leading to the fragmentation of the molecule.

Three prerequisites need to be met for IVR to be successful, otherwise the absorbed IR photon will simply be re-emitted. Firstly, the density of 'dark' states needs to be large enough. If there are not enough states at the same energy of the accepting mode, IVR will limit the excitation rate. Second, the coupling between these states (*i.e.* the anharmonicity) needs to be strong enough. Third and last, the laser used for this transition needs to ensure that multiple absorptions can occur within a laser pulse. The best tool for this is the free-electron laser, which will be introduced in Chapter 3.

Dissociation energies of C–H bonds in from fully aromatic PAHs are 4.5 eV, making these molecules notoriously difficult to fragment. When the fluence of the (free-electron) laser is not high enough to achieve fragmentation, an intense, non-resonant laser can be

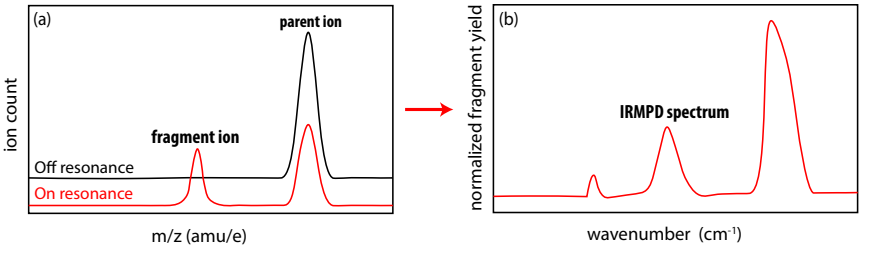

FIGURE 2.4: Illustration of IRMPD spectroscopy. A tuneable high-intensity IR laser is used to irradiate ions to the point of dissociation. a) Mass spectra. Off resonance, only the parent ions are present (black curve). On resonance, fragment ions appear (red curve). b) Illustration of an IR spectrum obtained by measuring the normalized fragment yield as function of laser frequency.

used to help, such as a high-power CO_2-laser [147, 148]. Shortly after resonant excitation, the vibrationally hot molecule can be heated with a highly intense nonresonant laser to reach the dissociation threshold. For successful use of this technique, the CO_2 laser intensity must be sufficiently low, so that it cannot fragment the ions without resonant pre-excitation.

The appearance of charged fragments, detectable with MS, is a signature of resonant IR absorption. This principle is laid out graphically in Fig. 2.4. The IRMPD spectrum can be found by monitoring the total fragment mass count N_{frag}, parent mass count N_{par} and power P as a function of the frequency ν, and then applying the subsequent formulas to find the normalized fragment yield $Y(\nu)$ [149]:

$$Y(\nu) = \frac{1}{P(\nu)} \ln\left(\frac{N_{\text{par}}(\nu)}{N_{\text{par}}(\nu)+N_{\text{frag}}(\nu)}\right), \quad \text{for} \quad N_{\text{frag}} \ll N_{\text{par}}, \tag{2.20}$$

$$Y(\nu) \sim \frac{1}{P(\nu)} \frac{N_{\text{frag}}}{N_{\text{par}}}. \tag{2.21}$$

Recent work has shown that the relation between the laser fluence and the normalized fragment yield is linear if saturation effects are avoided and fragmentation below the lowest measurable mass is limited [150]. For experiments where the laser produces highly intense light, and highly excited molecules can fragment into particles smaller than the mass spectrometer's lowest measurable mass, extra caution needs to be taken in directly comparing experimental spectra to theoretical spectra or spectra obtained from interstellar observations.

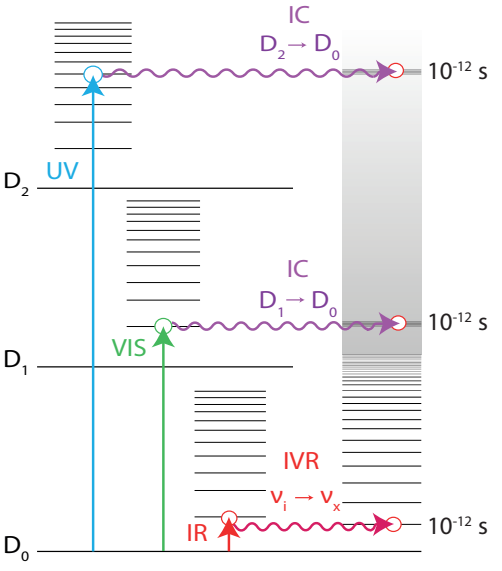

FIGURE 2.5: A Jablonksi diagram, showing the D_0, D_1 and D_2 states of a cationic PAH molecule, and their vibrational manifolds. The open bullets show which state is occupied. The straight arrows depict radiative energy transfer, whereas the wavy lines depict non-radiative transfer. On the right, the vibrational states of D_0 are depicted at excitation energies higher than the excitation energies of higher-lying electronically excited states. Timescales for these processes are equal on the order of ps and faster.

2.3 Ultraviolet photodissociation

IRMPD spectroscopy reveals different fragmentation channels along with the spectra, providing insights in the potential energy landscapes of the studied molecules. Like for IR spectral comparison, caution needs to be taken when putting the results from IR fragmentation mass spectra of PAH into astronomical contexts, due to the inherently different nature of interstellar UV photodissociation processes. We will briefly explain how these processes are different.

In Fig. 2.5, a diagram is shown of the electronic states in a cationic PAH with a doublet ground state. UV/Vis photons (blue and green) excite the molecule to a higher electronic state (D_1 or D_2), and this energy can then be transferred to a highly excited vibrational state in the electronic ground state D_0, in a rapid internal conversion (IC) process ($\sim 10^{-12}$ s) [151]. The vibrational energy is redistributed through intramolecular vibrational redistribution (IVR) at a similar timescale, and then released through IR radiation (~ 1 s) from various vibrational states, which we detect as the AIBs [7, 43].

When the supplied energy is above the dissociation threshold the molecule undergoes IC and IVR, and is then most likely to lose hydrogen atoms [7, 43]. Through UV excitation and subsequent mass spectrometry in the laboratory, reaction mechanisms governing critical interstellar photodissociation processes can be studied [88, 137–139, 152]. In the case of IRMPD, the internal energy is built up from the vibrational ground state. Although the time scales are comparable, fragmentation channels with lower energies could be favored due to the incremental rise in internal energy. Both of these methods are used for the determination of the D/H ratio in aliphatic hydrogen groups in Chapter 4, as they provide complementary information.

2.4 Computational methods

Quantum chemical predictions of PAH spectra have always been central to interpretations of interstellar spectra. By using numerical methods to solve the SE, it is possible to find accurate spectra for whole ensembles of molecules, which can be used to approximate the contents of interstellar clouds based on their emission spectra. Furthermore, as much as the development of theory leans on laboratory benchmarking, the laboratory experiments in turn lean on computational chemistry to support, interpret, and guide experimental findings. The most common quantum chemical method to predict the potential energy surface and IR spectral properties of large molecules is Density Functional Theory (DFT). A brief explanation of the general principles will be given here, for more detailed reading, the reader is referred to [153]. All calculations performed for the work in this thesis have either been done with the Gaussian09 [154] or Gaussian16 [155] software suite. Visual inspection of the calculated modes and structures was performed using the Chemcraft program [156] and the open-source software suites Avogadro [157] and Gabedit [158].

2.4.1 Fundamentals of density functional theory

The calculations presented in this work begin by finding the ground state geometry for the molecule. This involves solving the SE using the Hamiltonian ($\hat{H}$), which contains the kinetic energies for the nuclei (T_n) and the electrons (T_e), and the potential energies coming from the Coulombic attraction between electrons and nuclei (V_{en}), the Coulombic repulsion between the electrons (V_{ee}), and the between nuclei (V_{nn}). For a molecule with N atoms, $R = \{R_l,\ l = 1,\ldots,N\}$ denotes the nuclear coordinates, and $r = \{r_i,\ i = 1,\ldots,P\}$ denotes the electronic coordinates:

$$\hat{H} = \hat{T}_n + \hat{T}_e + \hat{V}_{ne} + \hat{V}_{ee} + \hat{V}_{nn}, \tag{2.22}$$

$$= -\sum_{l}^{N} \frac{\hbar^2}{2m_l}\nabla_l^2 - \sum_{i}^{P} \frac{\hbar^2}{2m_e}\nabla_i^2 - \frac{1}{4\pi\varepsilon_0}\sum_{l}^{N}\sum_{i}^{P} \frac{e^2 Z_l}{|R_l - r_i|} + \frac{1}{4\pi\varepsilon_0}\sum_{i=1}^{P}\sum_{j\neq 1}^{P} \frac{e^2}{2|r_i - r_j|} + \frac{1}{4\pi\varepsilon_0}\sum_{l=1}^{N}\sum_{m\neq 1}^{N} \frac{e^2 Z_l Z_m}{2|R_l - R_m|}. \tag{2.23}$$

The Born-Oppenheimer approximation is applied to this Hamiltonian, which means that the heavy nuclei are seen as immobile compared to the much lighter electrons. For minimum energy calculations, this automatically discounts the T_n term, because we assume $|R_l - R_m|$ to be constant. The wave functions and operators are now be rewritten as:

$$\psi(R,r) = \psi_e(r;R)\,\psi_n(R), \tag{2.24}$$

$$H(R,r) = H_e(r;R) + H_n(R), \tag{2.25}$$

and thus,

$$H_e(R,r)\,\psi_e(R,r) = E_e\,\psi_e(R,r), \tag{2.26}$$

$$H_n(R)\,\psi_n(R) = E_n\,\psi_n(R). \tag{2.27}$$

For any given configuration of the nuclei, the electronic SE can be solved, making it easier to find a geometry with a minimum energy with a step-by-step strategy. In DFT, instead of solving for all of the electrons, a key variable called the electron density $n(\vec{r})$ is defined for a system with P electrons:

$$n(\vec{r}) = P\int d^3\vec{r}_2 \ldots \int d^3\vec{r}_P\,\psi^{\dagger}(\vec{r},\vec{r}_2,\ldots,\vec{r}_P)\,\psi(\vec{r},\vec{r}_2,\ldots,\vec{r}_P).$$

For every operator contributing to the Hamiltonian, α ($\hat{T}_e, \hat{V}_{ne}, \hat{V}_{ee}$), and longer-range potentials, an energy density $\varepsilon_\alpha[n(\vec{r})]$ and corresponding energy E_α is defined, calculated locally at a value assumed by the electron density at every point in space:

$$E_\alpha[n] = \int n(\vec{r})\varepsilon_\alpha[n(\vec{r})]d\vec{r}.$$

$E_\alpha[n]$ is a functional, *i.e.* a function of a function. The way the different components of the Hamiltonian are approximated define how a DFT method performs for different molecular systems, and which energies are calculated with greater accuracy. A basis set is chosen to describe $n(\vec{r})$, treated in terms of distribution over different valence orbitals. Both the functional and basis set will have a large influence on the trade-off between computational accuracy and cost.

For PAHs, the B3LYP functional [159, 160] has been the workhorse for most calculations [99], and with great success. It performs well in spectral predictions, but other

functionals perform better for ground-state energy predictions. To that end we used the Minnesota functional, M06-2X. This choice was motivated by the improved accuracy of M06-2X in predicting barrier energies and relative energies of isomers with respect to B3LYP [161].

Most often, these functionals are combined with the 6-311++(2d,p) basis set [162], or a slight variation thereof. These basis sets account for the electron densities associated with covalent bonding, but not with influences of long-range, dispersive effects such as Van der Waals bonding. The chosen functional should also be able to produce this additional long-range potential if needed, as occurs for example in the case of noble gas-tagged molecules. Such corrections are implemented using, amongst else, by Grimme's D3 correction scheme [163].

2.4.2 Harmonic frequency calculations

Once the geometry of the ground state is optimized, it is possible to study the vibrational frequencies, calculating the force constant matrix (Eqn. 2.14) and diagonalizing it (Eqn. 2.16). The individual line positions are calculated in cm^{-1} with corresponding integrated absorption cross sections in $km \cdot mol^{-1}$. The theoretical stick spectra are convolved with a Gaussian line shape with an FWHM that simulates the spectral widths in the observed spectrum. Due to anharmonic effects, the experimental spectrum could be redshifted with respect to the theoretical predictions, which can be corrected for by implementing an artificial scaling factor on the predicted vibrational frequencies, ranging between approximately 0.940 – 0.983 ([131] and [164], respectively), chosen to match the calculated lines to the measured spectrum.

2.4.3 Transition states

Vibrations as they were described before are local minima of $V(R)$, and using this potential energy surface (PES), it is also possible to find saddle points. These saddle points are the transition states (TS) connecting PES minima, *i.e.*, different conformers. The frequency calculation or vibrational spectrum of a TS is characterized by having only one imaginary frequency (negative force constant k), which indicates that the energy has a maximum in only one direction (which is along the reaction path) [165]. The energy shows a minimum in the other (orthogonal) directions. Figure 2.6 shows a 3D representation of such a potential energy surface, where the saddle point is denoted by the white dot in the middle, and the two minima on either side represent both conformers, connected through the saddle point.

To find a TS, it is most helpful to have an educated guess of the TS structure. If no educated guess can be made, an alternative guess can be provided by stepwise changing the bonds involved in forming the other conformer. At each of these steps, the geometry is optimized and frequencies are calculated at a low-level basis set to reduce computational costs. When the TS is found, the calculation is repeated at a higher level, preferably

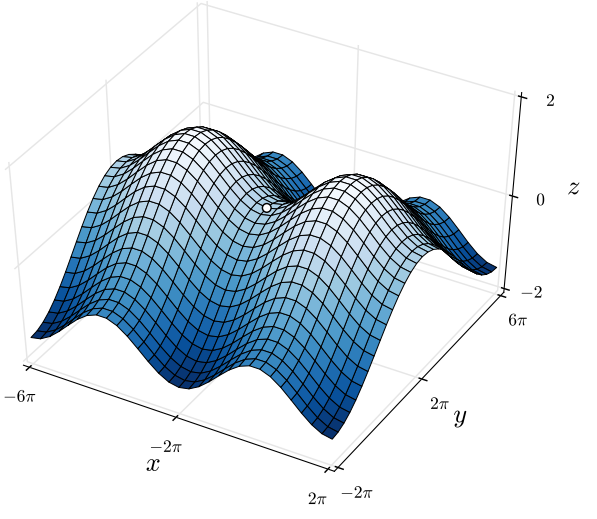

FIGURE 2.6: A potential energy landscape with two maxima, a saddle point – denoted by the white dot, and minima on the either side of the y axis. Credit to Wikipedia user Nicoguaro, re-use under Creative Commons Attribution 4.0. [166]

with a functional optimized for energy calculations, such as M06-2X. Finally, an intrinsic reaction coordinate calculation is performed to make sure that this maximum is connected to minima on either side, by moving through the minimum energy reaction pathway.

2.4.4 Anharmonic calculations

With the growing accuracy and sensitivity of the available laboratory methods, deviation from the scaled harmonic spectra becomes more evident. By including the cubic and quartic terms of the Taylor expansion for vibrational displacement (see Equation 2.18), it is possible to compare the measured spectra to unscaled theoretical predictions, and explain features that were not predicted in the harmonic predictions [143, 167–171]. As the anharmonic terms involve the treatment of three- and four-dimensional K-matrices (following the method in equation 2.16), the computation of anharmonic spectra can become very computationally expensive for an increasing number of atoms N. The functional and basis set must be carefully considered to minimize the computational cost.